

# Vibration-Based Diagnostics for Rotary MEMS

Jeremy Feldman, Brendan Michael Hanrahan, Saswat Misra, Xiao Zhu Fan,  
Christopher Mike Waits, *Member, IEEE*, Paul D. Mitcheson, *Senior Member, IEEE*,  
and Reza Ghodssi, *Fellow, IEEE*

**Abstract**—This paper demonstrates the use of low-cost off-the-shelf (OTS) microelectromechanical system (MEMS) technology to perform vibration-based *in situ* monitoring, diagnostics, and characterization of a MEMS microball bearing supported radial air turbine platform. A multimodal software suite for platform automation and sensor monitoring is demonstrated using a three-level heuristic software suite and sensor network. The vibration diagnostic methods used in the platform have applications in rotary microsystems for the early detection of failure, fault diagnosis, and integrated diagnostic systems for feedback-based optimization to increase device performance, reliability, and operational lifetimes. The studied rotary microdevice used a dual OTS accelerometer configuration for dual range parallel redundant vibration analysis. The sensor suite has been used to monitor and detect multiple operational parameters measured optimally in time or frequency domains such as rotor instability, imbalance, wobble, and system resonance. This paper will lay the framework for active diagnostics in future MEMS devices through integrated systems. [2014-0236]

**Index Terms**—Non-destructive testing, rotating machine measurement, rotating machine stability, vibration measurement.

## I. INTRODUCTION

VIBRATION is a characteristic of all machines and has long been known to be a product of all mechanical rotary systems due to imperfections in design or manufacturing [1]. In macroscale machinery, rotary machines use rolling element bearings to provide low friction and wear contacts for two surfaces with relative velocity while under load. The stiffness and geometric accuracy of the rolling element bearings contribute to the vibration characteristics of rotary machines, and therefore, vibration monitoring provides insight into the mechanical state of the bearings. Microscale rotary machinery also uses different kinds of bearings and will have a set of state-specific vibration signals.

Manuscript received August 4, 2014; revised November 12, 2014; accepted November 26, 2014. Date of publication January 13, 2015; date of current version March 31, 2015. This work was supported by the U.S. National Science Foundation under Award 0901411. Subject Editor C. Rembe.

J. Feldman, S. Misra, X. Z. Fan, and R. Ghodssi are with the Department of Electrical and Computer Engineering, Institute for Systems Research, University of Maryland, College Park, MD 20742 USA (e-mail: jerplane@gmail.com; smisra8@terpmail.umd.edu; xiaozfan@gmail.com; ghodssi@umd.edu).

B. M. Hanrahan was with the Department of Materials Science and Engineering, University of Maryland, College Park, MD 20742 USA. He is now with the U.S. Army Research Laboratory, Adelphi, MD 20783 USA (e-mail: brendan.m.hanrahan.ctr@mail.mil).

C. M. Waits is with the U.S. Army Research Laboratory, Adelphi, MD 20783 USA (e-mail: christopher.m.waits.civ@mail.mil).

P. D. Mitcheson is with the Department of Electrical and Electronic Engineering, Imperial College London, London SW7 2AZ, U.K. (e-mail: paul.mitcheson@imperial.ac.uk).

Color versions of one or more of the figures in this paper are available online at <http://ieeexplore.ieee.org>.

Digital Object Identifier 10.1109/JMEMS.2014.2383171

Vibration-based diagnostics consist of a vibration-to-signal transduction followed by computational analysis, allowing for diagnosis and prognosis of faulty operation or failure prevention. There are two main threads of vibration analysis, the first dealing with whole body motion and the second with pressure waves that propagate through a body [2]–[7]. These mechanisms are analyzed in either the time or frequency domain, depending on the characteristics of the vibration source. In whole body motion, the body is assumed perfectly rigid, and hence, the entire body is assumed to move as a rigid mass, whereas in a pressure wave vibration, the body is not rigid and waves will propagate through the entire body from their point of origin. Waves that propagate through the solid originate from a single point and travel outward at roughly the speed of sound through that material. Pressure wave vibrations are detected more effectively using time domain analysis and are seen as impulses at a much higher frequency than whole body motion vibrations [1]. Whole body motion vibrations are best analyzed using both time and frequency domain methods [1], [5]–[7].

Time and frequency domain methods for vibration diagnostics have been studied extensively and methods demonstrated successfully in literature comprise the shock pulse method (SPM), observation of periodic time domain peaks, measuring the overall root-mean-square (RMS) level and crest factor, system component specific resonances, and defect specific periodic vibrations characteristic of certain defects [2]–[5]. SPM is a method used successfully in literature and in industry to detect and count time domain impulses due to dynamic surface interaction [5], [8], [9]. Measuring overall RMS vibration aids in characterization and overall condition assessment, but has had limited success in detection of localized defects [5], [7], [10]. The observation of periodic time domain peaks has been shown to successfully detect local defects caused by interactions between mating elements that occur at a single point in the raceway and repeat every revolution [5], [11]–[13]. In the frequency domain, the occurrence of system resonances appearing as peaks in the fast Fourier transform (FFT) over a selectively filtered dynamic range and causing excitation of natural frequencies can be successfully correlated with assumed defect modes [5]–[7], [10], [14]–[18]. Additionally, it is notable that periodic peaks in the time domain are more effectively detected in the frequency domain as a peak in the FFT, with specific peaks in some cases consistently acting as a marker of specific defects [5], [17]–[19]. Generally their techniques rely on human interpretation, although some work exists on automating the detection process [5], [20], [21].

Automated detection has clear advantages and is required for integrated diagnostic schemes. Although these characteristics and techniques have been explored in great detail in macroscale machinery, very little has been done to translate these benefits to rotary MEMS.

In this paper, techniques are presented to aid in the understanding of microscale tribology by translating successful macroscale vibration diagnostic techniques to their microscale counterparts realizing benefits such as improved microsystem reliability, predictability, longer lifetimes, and overall improved performance with the term “higher performance” defined as higher rotational speed per unit input power. The research discussed herein demonstrates a vibration diagnostics suite for a rotary MEMS device (RMD) supported on micro-ball bearings with integrated accelerometers. Variations of both time and frequency domain analysis are used on time synchronous data collected from a suite of sensors, defined herein as the “sensor suite.” A collective set of Labview and MATLAB programs are used to automate the platform, perform the necessary signal processing and record data, and are referred to herein as the “software suite.” The software suite uses a heuristic approach for enabling high level detection of specific non-optimal or potentially damaging operational characteristics such as micro-ball whirl, rotor imbalance, turbine instability, and rotor wobble. This work uses OTS MEMS accelerometers (MA), due to their sensitivity, bandwidth, volume, and cost, to perform vibration analysis on a MEMS micro-turbine supported on stainless steel micro-ball bearings. For the first time, the dynamic characteristics of the micro-ball bearings have been elucidated using an OTS MA in conjunction with a suite of auxiliary sensors. On-chip vibration diagnostics provide a mechanism to improve the reliability of RMDs for future power, actuation, or sensing applications.

A set of operational characteristics from macroscale dynamics of rotary machines was expected on the microscale, but as of yet has not been demonstrated in a practical system. These macroscale characteristics consist of dynamic movement of the micro-balls, dynamic movement in the rotor due to fabrication tolerances, and dynamic surface interactions between the balls and the raceway. Due to the turbine design, it is expected that the dynamic nature of the micro-balls will cause sub-fundamental frequency components from clumping and also contribute to certain operational regimes where the balls either are held in place between the top and bottom raceway or are pushed to ride against the sidewalls as well due to centripetal forces. Certain tolerances in the fabrication are expected to show up as movement in either a vertical or horizontal fashion during operation relating to either raceway waviness or the viscous nature of the air bearing. The surface interaction theory is based on macroscale SPM and observes the changing dynamic changes in roughness of contacting surfaces and relates to wear. Monitoring these characteristics is critical to managing the reliability and performance of such devices. The results are presented in two categories: *time domain* and *frequency domain* detections. The defects detected in *time domain* device characterizations are those with a corresponding detection or observation occurring on low-level time domain samples. The defects detected in

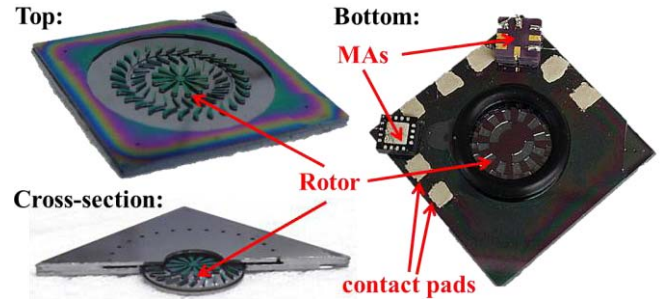


Fig. 1. Photographs: multiple device views. Bottom view showing the dual MEMS accelerometer (MA) configuration and contact pad configuration.

*frequency domain* device characterizations are those with a corresponding detection or observation occurring on intermediate level frequency domain samples. The device used for these tests is a MEMS rotary micro-turbine supported on micro-ball bearings with some characteristics specific to this device, and others applicable across all rotary microsystems.

## II. EXPERIMENTAL SET-UP

### A. Testing Platform

The RMD used in this study platform is a silicon MEMS micro-turbine supported on micro-ball bearings of  $285\ \mu\text{m}$  diameter (Fig. 1). The development of the micro-turbine is presented in [22], while characterization of the device is presented among [23]–[25]. The RMD is fabricated using a 45-five step, 14 photolithography mask microfabrication process. Deep-reactive-ion etching (DRIE) is employed throughout this process to define the ball bearing raceways, bond alignment, and turbine structures. DRIE allows for high-aspect-ratio, anisotropic silicon etching with tight tolerances and a scalloped surface morphology. The raceways in various RMDs are packed with a low packing (75%) or high packing (95%) density of micro-balls, allowing different spacing’s between each ball in the raceway. The wafers are mechanically aligned prior to subsequent thermo-compression bonding of the two components, with bond misalignment and bond quality being possible sources of defect. The RMD is composed of a three-wafer stack; two are bonded to form the rotor-stator assembly and a third wafer acts to direct turbine actuation gas flow.

A cross-sectioned schematic of the ball housing is presented in Fig. 2 to show both the dimensions of the bearings and the critical forces within the bearing. A thrust force ( $F_{\text{thrust}}$ ) acts upon the rotor and helps to maintain correct dynamic orientation, translating to the normal force seen by the ball ( $F_N$  in Fig. 2). During actuation, the normal force creates contact between the rotor, ball, and stator holding the riding points on the top and bottom of the ball. Another important force is the centripetal force acting on the ball ( $F_C$  in Fig. 2) during operation, which is perpendicular to the axis of rotation of the rotor. The ratio of  $F_N$  to  $F_C$  determines the dynamic characteristics of the ball rotation and is discussed in following sections.

The rotor-stator assembly has two MAs bonded directly to the stator. The first MA (*Analog Devices: ADXL 325*)

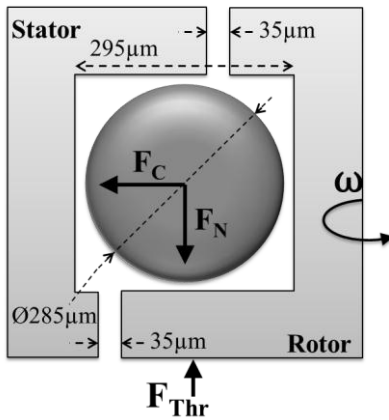


Fig. 2. Cross-sectioned schematic of the RMD showing rotor, stator, balls, and the axis of rotation of the device. Zoom shows a dimensioned ball bearing within the etched housing and the action of forces on the ball.

is used for high-sensitivity measurements with a sensitivity of  $174 \text{ mV/g}$ , a range of  $\pm 5 \text{ g}$ , and a bandwidth of  $0.5 - 1600 \text{ Hz}$ . The second MA (*ADXL001*) extends the range of the vibration study at the expense of sensitivity. The sensitivity, range and bandwidth of this device is  $16 \text{ mV/g}$ ,  $\pm 70 \text{ g}$ , and  $0.5 - 22000 \text{ Hz}$ , respectively. The electrical contact pads are silkscreened directly onto the stator with silver paste as a low temperature alternative to soldering to reduce thermal shock on the eutectic bonding layer between the two halves of the rotor-stator structure. The packaging for the micro-turbine was machined from a clear acrylic base-material comprising a bottom plate, a top plate, an electrical feed through plate, and connections for gas and pressure transducers. The packaging allowed for simultaneous, independent control of the normal load on the bearings, and rotor actuation with mass flow control [24].

### B. Sensor Suite

The various sensors used in the sensor suite are described detailing their location in the platform (Fig. 3). The turbine pressure sensor is used to measure the pressure at the turbine inlet and gives a reading of the pressure drop across the turbine assuming the outlet is at ambient pressure. The thrust pressure sensor is used to measure the pressurized cavity behind the rotor opposite the exhaust (thrust gas flow region in Fig. 3) and used to calculate the normal force applied to the rotor. The first optical displacement sensor (ODS) measures the distance to a surface on the rotor and is positioned above the rotor petals (Fig. 1) measuring a pulse every time a petal passes underneath the sensor to obtain rotor speed. The second ODS is used to measure the out of plane displacement at a single point above the rotor to extract wobble in the rotor. The mass flow controller is used to monitor and control the flow rate of the turbine actuation gas, thus controlling the rotational speed. Two accelerometers are used for vibration measurement. The RMD was designed to seat two accelerometers bonded to the stator with epoxy.

The dual accelerometer configuration was used for a wide measurement range, sensitivity, and bandwidth when operated

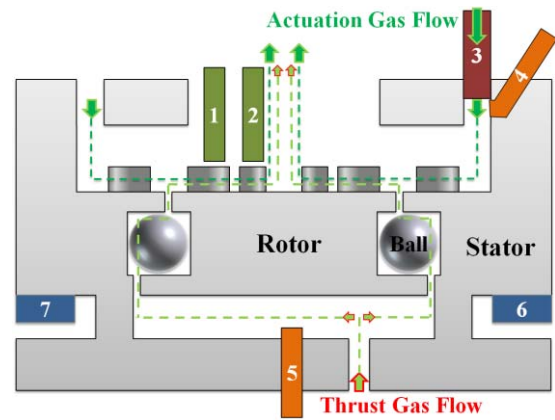


Fig. 3. Schematic packaging and sensor suite for the micro-turbine. The parallel set of collected samples consisted of samples from two [Philtec D6-H1] ODSs (1 and 2), MKS 1479A mass flow controller (3), [Philtec D6-H1] turbine and thrust pressure sensor (4, 5), and two accelerometers: a  $\pm 5 \text{ g}$  1700 Hz bandwidth ADXL325 accelerometer and an  $\pm 70 \text{ g}$  20 kHz bandwidth ADXL001 accelerometer (6 and 7).

in parallel. Above 5 g, the high sensitivity accelerometer saturates and its output is ignored. The sensor suite was calibrated and characterized, and was subsequently linear with datasheet expectations. Each sensor was independently tested with a known input signal to give an output signal and match values with expected values calculated from each OTS components specifications or test values from manufacturer provided datasheets. In addition to the independent sensor characterization, testing was performed after every sensor was integrated, reproducing each independent input-output relationship from independent testing. Along with the characterization of all OTS components, all sensors are initialized at the start, and linearity is confirmed. All sensors were connected to a LabVIEW DAQ NI-USB 6356 for acquisition. The NI-USB 6356 enabled multi-channel, simultaneous, independent sampling for time-synchronized sampling of platform sensors.

### C. Software Suite

LabVIEW based programs composed the bulk of the software suite, and managed the DAQ automation and most of the signal processing. MATLAB was used for later stage analysis and visualization on datasets exceeding the memory capabilities of LabVIEW. The device packaging, test platform, and sensor suite were realized with eight sensors operating in parallel at sample rates of 50K samples per second and managed by the software suite. An overview of the data processing flow and operation is shown in Fig. 4. LabVIEW software manages the platform by controlling the simultaneous sampling DAQ, controlling the mass flow controller and actuation gas shutoff valve, which actuates the MEMS micro-turbine. Time parallel (not multiplexed) samples are shifted into onboard registers before samples are obtained by LabVIEW in array form for signal processing Fig. 4(d). The most important operation of the software suite and sensor suite is the parallel management of the sensors, enabling time synchronized data acquisition, management, processing, and

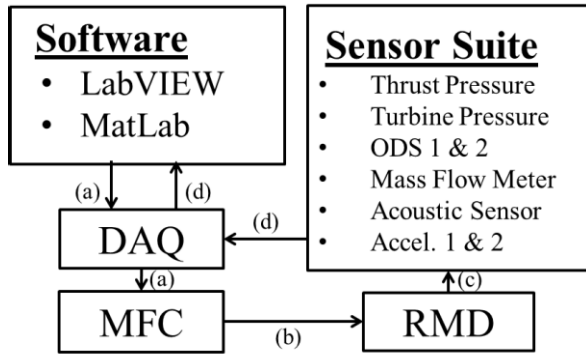


Fig. 4. System level overview of the diagnostic platform and operation. LabVIEW was used for automation, data recording, and processing. The DAQ was used for bridging the MFC and the sensor suite, the MFC was used for actuation gas management, the MEMS micro-turbine was at the heart of the platform, the sensor suite took all measurements and fed them back to the DAQ and then LabVIEW where data is processed and recorded with further analysis done with MatLab. Block flow labels are broken down into: control (a), actuate (b), characteristic transduction (c), read signal (d).

recording for each data set while simultaneously automating device actuation. Data fusion is used to resolve heuristics, and for the scope of this paper, the signal processing design for the software suite will be simplified to the three fusion data levels for discussion: low level, intermediate level, and high level.

This three-level data processing breakdown comprises raw samples at the low level in array form as the program handles eight of these arrays simultaneously. The intermediate level will categorize all raw samples post processed into FFT arrays calculated from raw sample arrays. The intermediate level deals primarily with the frequency domain and subsequent array based processing such as wobble and its FFT. The high level provides a detection scheme that is either passed to the user interface or used as feedback for another high-level detection scheme.

### III. RESULTS

#### A. Time Domain

1) *Rotor Wobble*: Rotor wobble is the physical out-of-plane displacement of the rotor and is due to fabrication imperfections in the form of raceway waviness but can also be worsened by improper loading or orientation of the bearing. Rotational sensors and actuators, which may be attached to or driven by a micro-turbine, need to accommodate for wobble when establishing sensitivity and operating parameters. For example, on-rotor optics intended for long-range sensing will be extremely sensitive to unintended out-of-plane movement. Similarly, rotary gyroscopes are inherently sensitive to tilt in the rotational axis. Therefore, measuring rotor wobble is important for rotary microsystems. Here, the out-of-plane movement of the rotor is monitored using an optical displacement sensor. Raceway depth has shown a 1-3 period/raceway frequency and amplitudes up to 800 nm. Excessive wobble can occur when insufficient normal load prevents the rotor from maintaining tight contact between the ball, rotor, and stator,

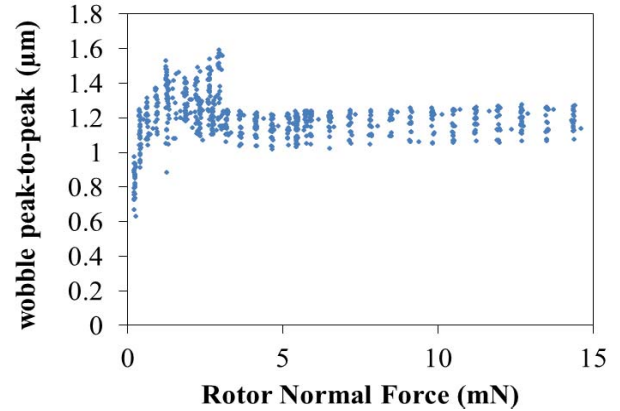


Fig. 5. Rotor wobble versus normal load, with low normal load wobble approaching  $1.6 \mu\text{m}$ , and higher normal load wobble settling at around  $1.2 \mu\text{m}$ .

causing fluctuations between two contact orientations and is not the same as raceway waviness. Tolerances allow for  $10 \mu\text{m}$  ( $\pm 600 \text{ nm}$ ) tolerance of vertical rotor movement (Fig. 2) with poor loading of the rotor at that point causing the rotor to wobble  $10 \mu\text{m}$  between the intended bearing surface and the opposite (point contact) surfaces. From these data, the minimum normal load is discovered to ensure minimum wobble operation, limited by raceway waviness. Fig. 5 shows the peak-to-peak wobble versus normal load for a single device. While the microfabrication of the silicon micro-turbine is not the focus of this paper, it is important to note a necessary asymmetry in the raceways as seen in fig. 2, and if a thrust force is not applied to the rotor ( $F_{\text{thr}}$  in Fig. 2), the balls will ride on the edges of the through-etched opening above and below the ball, whereas if a normal force is applied to prevent this, the balls will ride against the flat surfaces above and below the balls. The rotor wobble data show that at low normal load ( $F_N$  in Fig. 2), the actuated load ( $F_{\text{thr}}$  in Fig. 2), and gravitation load are nearly balanced so the rotor flutters between the two bearing orientations. Once the actuated load exceeds gravitational load, the rotor settles to a  $1.2\text{-}\mu\text{m}$  peak-to-peak operation, as shown in Fig. 5. The steady-state wobble is due to the fabrication dependent non-uniformity of the raceway and is expected to improve for smaller radius devices.

Wobble is more easily identified in a time domain data set, observed in low-level samples captured from an ODS and since the ODS measures optical displacement from the surface, out-of-plane motion can be measured. It is notable that wobble did not contribute significantly to out-of-plane vibration measured by the out-of-plane accelerometer axis as little correlation was observed. Once the program obtains a peak-to-peak measure of wobble, the software then compares the wobble to historical values over successive test cycles. Unusually, high wobble detection can be a marker of improper normal force loading or a damaged device.

2) *Turbine Instability*: The radial vibration of the device is monitored through a range of operating speeds and normal loads to explore intrinsic stability behavior of the turbine. Due to the process-specific planar geometry of the device, dynamic

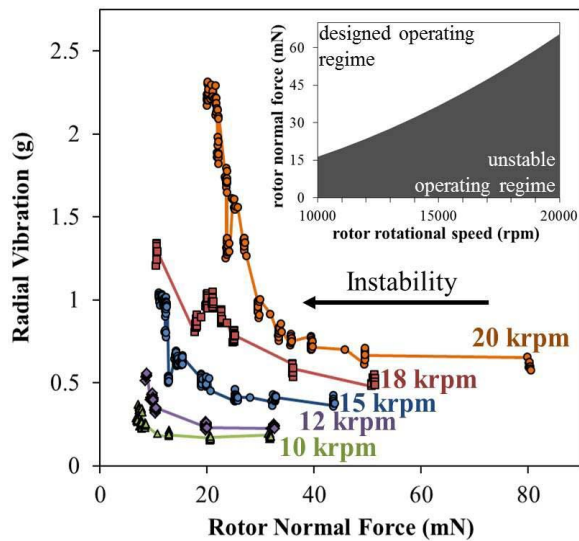


Fig. 6. Bearing stability showing different normal force loads on the bearing versus radial vibration amplitude for different rotational speeds. As the rotor normal force for a given speed is reduced, a parabolic relationship between radial vibration and rotor normal force occurs, and (inset) a transition region can be seen as calculated from theory between the two stability regimes.

stability becomes largely dependent on operational speeds inducing centripetal forces in the micro-balls with normal loads acting as a stabilizer. Bearing instability occurs in all macro- and microscale rotary devices but it is most prevalent on the micro level due to, for example, fabrication related raceway waviness due to imperfection. This phenomenon isn't just limited to ball bearing technology as indicated by Frechette *et al* [26] that aerodynamic properties of the bearing journal and thrust region produce instability in a micro-turbine supported on levitated bearings. For ball bearing devices, the primary cause of instability is due to the geometry of the device, fabrication of the bearings, and dynamic forces. When the micro-turbine rotor is actuated, angular velocity encourages the balls to move away from the center of the device, eventually overcoming the normal force grasp on the micro-balls in track, and the micro-balls will ride along or interact with the sidewalls of the bearing. This centripetal force is proportional to the square of the rotational velocity of the rotor. Adjusting the normal force on the rotor increases this sliding friction, maintaining the intended position of the balls within the center of the raceway. When the balls interact with the sidewalls, the device tends toward instability, indicated by the measured RMS radial vibration, which can be seen in fig. 6 showing radial vibration scaling with decreasing rotor normal force for different rotational speeds. As rotor normal force is reduced for each speed, there is a transition curve observed wherein the RMD crosses over into a less stable operation regime.

Permanent damage to the device has been shown to occur if left to run in this unstable regime. In order to counteract this centripetal force that leads to instability, a sliding friction force is needed to balance the radial force. This is achieved by increasing the rotor normal load (Fig. 2). The tradeoff to excessively high loads is accelerated wear in the raceway,

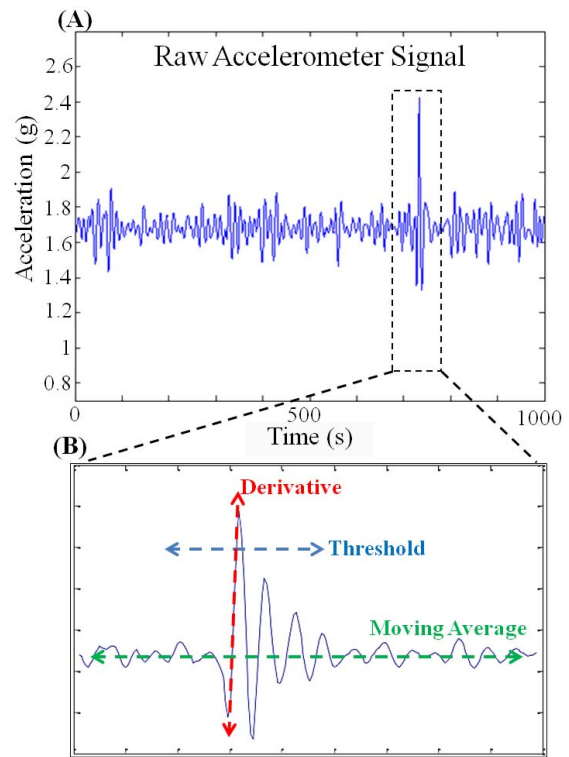


Fig. 7. (a) Accelerometer signal showing ball impact events and (b) time domain analysis.

which leads to higher friction and early device failure. By tuning the rotor normal load, counteraction of centripetal forces with a stabilizing normal load leads to an ideal operating mode and tracks the parabolic stability curve shown in the inset of Fig. 6 on the stable side. This allows for the selection of certain parameters of speed and load that best optimize turbine performance without significant degradation.

3) *Ball Impact Events*: In macroscale rotary machines, ball bearings use a retainer ring that maintains a constant spacing between each ball between the bearings inner and outer race, and maintains both the ball-to-ball spacing and the spacing between the ball and raceway walls. Due to the complexities of scaling down to the microscale, a ball bearing separator bracket is not used, so balls are free to re-distribute, rub against, or impact with other balls [27]. Additionally, the tolerances of the raceway dimensions allow for some radial ball movement in the direction of centripetal force. Since the balls and rotor have the freedom to move about during operation, it is reasonable to assume that impulse type events are detected in the time domain data from the accelerometer. The impulses will be referred to herein as a “ball impact” and are characterized as a sudden spike in the accelerometer signal (Fig. 7A), caused by either a ball-to-ball interaction, or a ball-to-rotor and raceway or another interaction in-between, with an example of one such ball impact shown in Fig. 7. It is believed that impulses like these over the lifetime of the device will correlate with device wear and eventual failure, although statistical analysis is needed for verification, ball impact detection and counting is a powerful addition to the current software suite and adds a new level of wear insight to

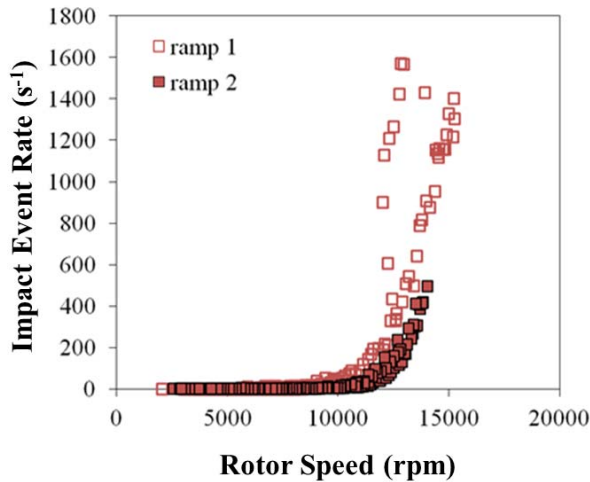


Fig. 8. Impact event rate over two successive ramp tests, showing a significant difference in impact rates.

the vibration diagnostics suite as it relates to the SPM methods discussed in section I.

Time domain analysis is used to detect and count each of these impulse events (on average) by using a combination of derivative and threshold cross in comparison with the moving average (Fig. 7B). An impact imparts a higher force at that point in time between two interacting surfaces, and therefore, may play a role in surface wear in the form of surface pitting, spall formation, and erosion [28], [29]. According to Wowk, these metal impacts or shock pulses do not necessarily indicate a faulty bearing, but they do indicate that a material-to-material impact is occurring due to defects, high loads, or a lack of lubrication, and are one of the earliest indicators of bearing wear [1], [5]–[7], [29]. As wear progresses, these shock pulses increase in number and severity and are a method for bearing analysis in that they look for and count the impacts or shock pulses [1], [30], [31]. With adequate filtering of high frequency electrical noise and shielding, these impulses can be detected, counted, and correlated to device age and performance for purposes such as operational optimization and failure prediction. When hard materials such as silicon are struck by steel balls, the relationship between the physical properties of the impacting particle and the impact surface determine the level of deformation or material removal due to the impact. This surface damaging action is partially due to the force imparted by the ball or shockwave, and the sudden heat change at the point of impact, which acts to erode ball and raceway material, as discussed in Oka et al. [28], [29].

Ball impact detection and monitoring over the lifetime of the device produces a second level of insight into the operation and characteristics of RMDs. This can be seen in Fig. 8, which shows an increase in the ball impact rate with increasing actuation power, as expected. The impulse rate versus input power for the device operating through a range of rotational frequencies clearly shows two different modes of operation, one with more ball impacts than the other, which is reflected in the differences in actuation power to reach the same rotational speed.

The RMD operating at 14 krpm required between 57–72 mW of actuation power, while the ball impact rate

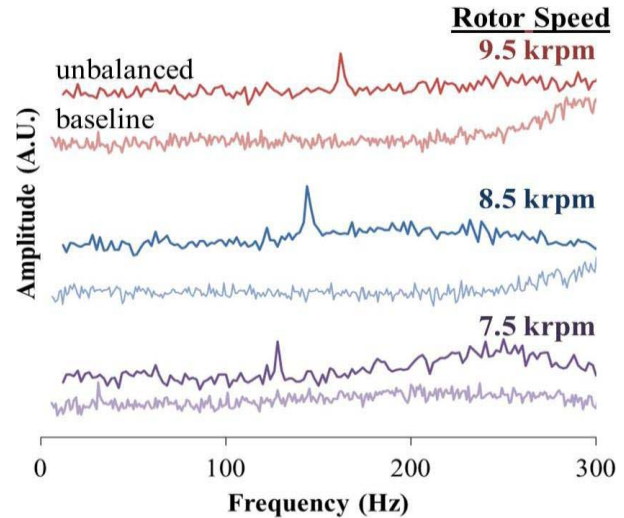


Fig. 9. Unbalanced bearing due to a weight offset: a defect manufactured by placing a micro-droplet onto one side of the rotor causing a shift in balance, and measured via the on-chip accelerometer.

varied from 493 to 909 impacts/sec during a whirl event, a 15% increase in power required and an 84% increase in impact rate was correlated directly to whirl damage. This result highlights the prognostic capability of monitoring ball impact events versus other data. Significant increase in impact event rates may have a predictive capability on the microscale as they do on the macroscale [28], [29].

### B. Frequency Domain

1) *Rotor Imbalance*: Micromachined rotors are very sensitive to fabrication-induced imbalances. The centripetal force imparted on the rotor is the product of the mass, radius, and angular velocity squared of a single defect. A minor defect on a low speed microscale device becomes significant at the speeds of 1Mrpm, which are intended for power-generating MEMS [32]. Such minor imbalances can arise from misalignment in bonding, lithography processes defects, and/or etch non-uniformities. Early detection of rotor imbalance is critical to preventing catastrophic device failure as it is accelerated to operating speeds. The accelerometer has been used to diagnose an experimentally unbalanced rotor. The micro-turbine is unbalanced by placing less than 1 milligram of polymer in a single location along the periphery of the rotor. For these tests, the rotor is operated at a set rotational speed and a time-averaged vibration spectrum is obtained. The imbalance is observed by taking the FFT of the accelerometer data to obtain the frequency spectrum and measure the magnitude of the fundamental vibration magnitude. A peak is observed corresponding to the rotor rotation rate, the fundamental frequency (1X), which is the rotor operating speed. This is seen in Fig. 9, where the appearance of the fundamental peak for an unbalanced rotor and the baseline measurement after the polymer is removed. To generalize the diagnostic capabilities, a sensitivity coefficient of  $0.0098 (m_i * r_i * \omega^2) / m_r$  is defined, where  $\omega$  is the rotor's rotational velocity,  $m_r$  is the rotor's mass,  $m_i$  and  $r_i$  are the mass and radius of the imbalance, respectively [24]. This correlates to a minimum sensed mass

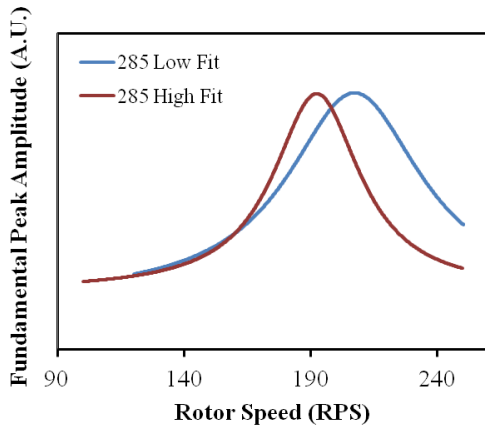


Fig. 10. Measured values of fundamental peak amplitude versus rotor speed for a 95% packing factor or 285 high (red Lorentzian fit), and a 75% packing factor or 285 low (blue Lorentzian fit) devices.

imbalance of  $0.2 \mu\text{g}$  at the periphery of the rotor spinning at 50 krpm.

2) *Rotor Resonance*: Rotor resonance is a characteristic of all rotary actuators due to excitation of natural frequencies causing resonance in the mass-spring-damper characteristics of the rotary actuator. In the RMD tested, resonance is present in the form of oscillations of the rotor. For these tests, the micro-turbine was actuated to speeds up to 20 krpm while the FFT of radial vibration for each speed was being recorded. Two devices with different ball bearing packing factors (75% and 95%) were actuated to detect a resonance shift due to the change in mass from a different packing factor. The RMS radial vibration with respect to the fundamental frequency given by the speed is shown in Fig. 10. Peaks were observed at 11.3 krpm for the 285 high fill factor device and at 12.2 krpm for the 285 low fill factor device. In the case of reducing the amplitude of resonance in the RMD, there are two options: alter the intrinsic spring constant of the system, or the more difficult option, use precision balancing to reduce the resonant mode excitation. Using the on-chip accelerometer, resonant modes in the RMD are measured by isolating an imperfection driven frequency component and tracking that component's vibration across the operational frequency range.

Information about bearing stiffness at the resonant speed can be determined from the resonance frequency of the rotor and the geometries of the system. This rotor/bearing mechanism can be modeled as a traditional harmonic oscillator. With this model, the spring constant of the 285 high device was calculated to be 6 N/m, given by  $\text{resonant freq} = \frac{(k/m_w)^{1/2}}{2\pi}$ , with spring constant  $k$ , and  $\frac{1}{2}$  rotor mass  $m_w$ . The low calculated spring constant means resonance comes from air perturbations within the bearing and not from ball-to-ball contact as the spring constant for a single stainless steel ball is at least an order of magnitude larger [33]. In verifying this resonance theory, devices were tested with a reduced ball density in order to create a small shift in the mass from an approximate 20 ball difference. A slight peak in the resonance in the correct direction is apparent in this test, seen in Fig. 10. Using the same model, with the same spring constant and new resonant peak, a mass change of roughly 0.6 mg was calculated.

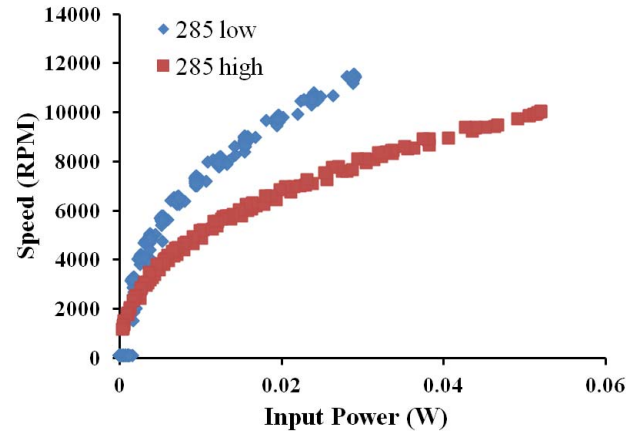


Fig. 11. Performance curves for two tested RMDs. Higher speed for the same power marks higher performance.

A single 440C stainless steel ball from the device weighed  $95 \mu\text{g}$ , and with a 75% (about 20 micro-balls) reduction roughly in line with this mass change calculated from the model, supporting the theory. When rotational frequencies match the mechanical resonance properties of the bearings, vibration amplitudes will exceed normal levels. Therefore if these resonant regions are known, the operating conditions can be altered to push through resonant regions to prevent resonance induced damage or premature failure. Alternatively, this technique can be used to evaluate different suppression methods that minimize the impact of resonance.

3) *Micro-Ball Whirl*: As previously discussed, in macroscale rotary machinery a retainer ring is often used to maintain a constant spacing between each ball between the bearings inner and outer race for high speed operation. For the RMD used in this diagnostic platform, a retainer ring is not used due to the lack of a microscale fabrication solution, allowing the micro-balls to freely adjust their spacing [27]. Two configurations of device were fabricated for demonstrating the relationship between rolling friction and dynamic performance. Friction has been theorized to scale with contact area, supported by the friction study presented by Hanrahan in [23]. Due to this property, it is expected that with fewer micro-balls a higher level of RMD performance is expected. Fig. 11 compares the performance of the two different ball packing densities. The 75% packing density shows significantly higher performance over the 95% packing density device.

Fig. 10 demonstrates the expected benefits of a low ball packing density, but as discovered from the vibration diagnostics of the low density device, the downside to this higher performance configuration is induced rotor whirl. Whirl in the RMD device is characterized as a dynamic clustering of the balls and is different from an imperfection-caused imbalance. This dynamic clustering occurs under certain operational conditions with a unique sub-threshold fundamental frequency domain marker, and is referred to as “ball whirl” (Fig. 12).

Ball whirl is specific to the low ball density devices because of the clustering of the balls during operation. When all of the balls are evenly distributed within the bearing raceway,

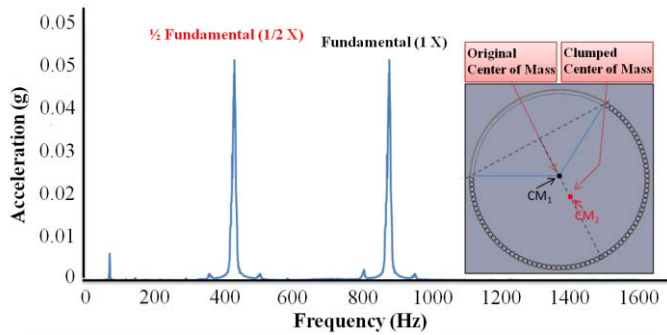


Fig. 12. Accelerometer FFT showing whirl mode operation. (inset) To-scale schematic depiction of 'ball whirl'. The rotor will shift to the stator in the point opposite to the clump of balls, though will not touch unless the raceway failure or breakage occurs. The 75% ball packing can create a significant offset and shift the center of mass of the balls as shown.

the total mass of all balls is evenly distributed. When the balls cluster together, then the total mass of the balls will be shifted to a new center of mass offset from the geometric center of the combined rotor and bearing system. This mass offset creates another excitation mode for the turbine corresponding to a 0.5X rotational speed. The rotor rotation rate is the fundamental frequency (1X) and the balls will translate around the raceway at one half times the fundamental frequency (0.5X). The grouped ball mass produces a clear frequency component that appears in the accelerometer spectrum at this 0.5X marker.

When ball whirl is detected, the device is operating in an unsafe regime with a greater sensitivity to rotor resonance modes. The early detection of ball whirl enables preventative measures to be taken as performance does not change when initially detected in a new device (Fig. 13A, 1902-2562 seconds), but continual operation of the device under this mode of operation will lead to damage and eventual catastrophic failure. Understanding the characteristics of whirl allow for optimization from a tradeoff between friction from the low number of balls and the lifetime change due to whirl when the number of balls is varied across different devices. Ball clustering occurs randomly, but may be influenced by factors such as speed or simply a slight offset of the planar orientation from horizontal causing gravity to pull balls to one side. Another theory is that ball clustering may occur partially due to centripetal forces momentarily overcoming the normal forces keeping the rotor in stable operation. Neither of these theories has been verified due to the complexity of interactions and the fact that ball clustering is not an operational regime that can be reproduced on command. The operation and detection characteristics are detailed in Fig. 13 showing the operational characteristics in Fig. 13A, and the detection characteristics in Fig. 13B along with the corresponding example of the marker seen in Fig. 13C.

Ball clustering or whirl presents a significant problem for devices designed for lower ball packing densities. With the performance benefit tradeoff being significant for a device with a lower ball packing density, finding a design to operate the device optimally and reliably for long periods of time is highly beneficial. Additionally, a device with a lower ball packing will be able to use the diagnostic system to prevent catastrophic

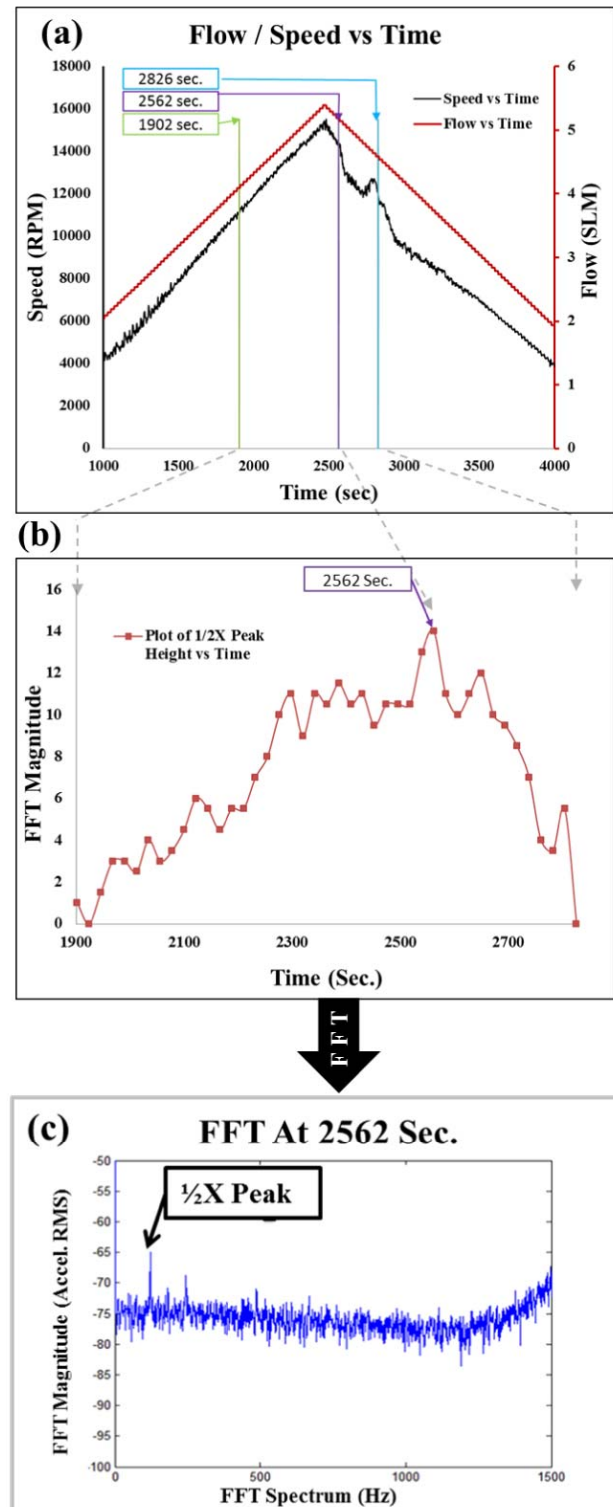


Fig. 13. Ramp testing of the automated input flow in red and output actuation response of the rotor (speed) in black. The 1/2X fundamental peak is first detected at 1902 seconds, then peaks out at 2562 seconds, and by 2826 seconds the 1/2X peak is no longer detectable (A). The figure shows the magnitude of the 1/2X peak height detected during detected time frame (B). The figure shows an example 1/2X peak within an accelerometer spectrum (C).

failure and resolve the optimal ball loading or operating conditions using the diagnostic capabilities to measure whirl and the conditions that cause it. The vibration diagnostics

system may act as a tool to study the different phenomena and optimize the design for a final device. Whirl can be detected well before damage or performance degradation occurs as seen in Fig. 13, with a notable detection occurring at 1,902 seconds and leading up to performance reduction at 2,562 seconds, giving a full 660-second window for the system to react to this detection of whirl.

Ball whirl detection uses an FFT driven approach as the  $\frac{1}{2}X$  peak is a reliable marker, and while the  $1X$  peak is seen in all devices due to intrinsic imbalance. The  $\frac{1}{2}X$  detection is not common, but does lead to accelerate device degradation and may potentially add to resonance inducing excitation, adding to damage caused by the  $\frac{1}{2}X$  peak and its resonance vibration. While it would be ideal to find preventative measures for ball whirl, prevention may not be possible.

#### IV. CONCLUSION

Rolling element bearing technology is well known and widely used in macroscale machines due to its low cost and high relative performance in comparison to air, fluid, or magnetic bearing technologies. As form factors scale from the macro- to microscale, the operational dynamics and performance regimes are not well known, with macroscale characteristics often not scaling in the same way as their microscale counterparts. As MEMS rotary systems mature and become more prevalent in commercial system design, a full understanding of characteristics in rotary MEMS, as well as methods to monitor these systems to guarantee reliable lifetime and performance, will be needed. This paper demonstrates the use of vibration analysis using integrated accelerometers to perform in-situ monitoring, diagnostics, and characterization for a MEMS rolling element ball bearing supported rotary turbine. A multimodal monitoring software suite was designed to interface with sensing transducers at the platform level allowing for monitoring, automation, and data collection. The monitoring suite enabled the implementation of heuristic methods to characterize different phenomenon. The accelerometer is shown to provide high sensitivity, and wide bandwidth measurement of the forces generated in the rotating micro-turbine. A dual accelerometer configuration is used to record vibrations at two different sensitivities ranges, when both are bonded to the micro-turbine stator and analyzed in parallel. Monitoring is performed using advanced multi-independent channel and time-synchronized sampling of each sensor. The sensor suite has been used to characterize the rotor instability for rotor speeds from 10-20 krpm, diagnose imbalance acceleration with sensitivity down to 0.001 g, determine rotor wobble with an accuracy of <500 nm, and monitor system resonances through the speed range of 5-30 krpm. The data provided by the system have applications in rotary microsystems for the early detection of failure, fault diagnosis, and integrated diagnostic systems for feedback-based optimization to increase device performance, reliability, and operational lifetimes.

#### ACKNOWLEDGMENT

The authors would also like to acknowledge the Maryland Nanocenter and the U.S. Army Research Laboratory Cleanroom Staff.

#### REFERENCES

- [1] V. Wovk, *Machinery Vibration: Measurement and Analysis*. New York, NY, USA: McGraw-Hill, 1991.
- [2] F. Cong, J. Chen, G. Dong, and M. Pecht, "Vibration model of rolling element bearings in a rotor-bearing system for fault diagnosis," *J. Sound Vibrat.*, vol. 332, no. 8, pp. 2081–2097, 2013.
- [3] I. Howard, *A Review of Rolling Element Bearing Vibration 'Detection, Diagnosis and Prognosis'*, document DTIC, 1994.
- [4] H. Rahnejat and R. Gohar, "The vibrations of radial ball bearings," *Proc. Inst. Mech. Eng., C, J. Mech. Eng. Sci.*, vol. 199, no. 3, pp. 181–193, 1985.
- [5] N. Tandon and A. Choudhury, "A review of vibration and acoustic measurement methods for the detection of defects in rolling element bearings," *Tribol. Int.*, vol. 32, no. 8, pp. 469–480, 1999.
- [6] N. Tandon and B. C. Nakra, "Comparison of vibration and acoustic measurement techniques for the condition monitoring of rolling element bearings," *Tribol. Int.*, vol. 25, no. 3, pp. 205–212, 1992.
- [7] N. Tandon and B. C. Nakra, "Detection of defects in rolling element bearings by vibration monitoring," *Indian J. Mech. Eng. Division*, vol. 73, pp. 271–282, Jan. 1993.
- [8] R. Alfredson and J. Mathew, "Time domain methods for monitoring the condition of rolling element bearings," *NASA STI/Recon Tech. Rep. A*, vol. 86, no. 6, p. 22166, 1985.
- [9] D. E. Butler, "The shock-pulse method for the detection of damaged rolling bearings," *Non-Destruct. Test.*, vol. 6, no. 2, pp. 92–95, 1973.
- [10] T. Miyachi and K. Seki, "An investigation of the early detection of defects in ball bearings using vibration monitoring—practical limit of detectability and growth speed of defects," in *Proc. Int. Conf. Rotordyn.*, Tokyo, Japan, 1986, pp. 14–17.
- [11] O. G. Gustafsson and T. Tallian, "Detection of damage in assembled rolling element bearings," *ASLE Trans.*, vol. 5, no. 1, pp. 197–209, 1962.
- [12] T. Igarashi and H. Hamada, "Studies on the vibration and sound of defective rolling bearings: First report: Vibration of ball bearings with one defect," *Bull. JSME*, vol. 25, no. 204, pp. 994–1001, 1982.
- [13] T. Igarashi and J. Kato, "Studies on vibration and sound of defective rolling bearings: Third report: Vibration of ball bearing with multiple defects," *Bull. JSME*, vol. 28, no. 237, pp. 492–499, 1985.
- [14] J. Broderick, R. Burchill, and H. Clark, "Design and fabrication of prototype system for early warning of impending bearing failure," NASA, Washington, DC, USA, Tech. Rep., 1972.
- [15] M. S. Darlow and R. H. Badgley, "Early detection of defects in rolling-element bearings," SAE Tech. Paper 750209, 1975.
- [16] K. F. Martin and P. Thorpe, "Normalised spectra in monitoring of rolling bearing elements," *Wear*, vol. 159, no. 2, pp. 153–160, 1992.
- [17] P. D. McFadden and J. D. Smith, "Model for the vibration produced by a single point defect in a rolling element bearing," *J. Sound Vibrat.*, vol. 96, no. 1, pp. 69–82, 1984.
- [18] P. McFadden and J. Smith, "Information from the vibration of rolling bearings," *Condition Monitor.*, vol. 84, pp. 178–190, Apr. 1984.
- [19] P. McFadden and J. Smith, "The vibration produced by a single point defect on the inner or outer race or rolling elements of a bearing under radial or axial load," Ph.D. dissertation, Dept. Eng., Univ. Cambridge, Cambridge, U.K., 1983.
- [20] J. MacIntyre, P. Smith, T. Harris, and A. Brown, "Neural network architecture and their application in condition monitoring," in *Proc. Condition Monitor. Diag. Eng. Manage. Conf.*, New Delhi, India, 1994, pp. 220–227.
- [21] S. M. Wu and C. J. Li, "On-line detection of localized defects in bearings by pattern recognition analysis," *J. Manuf. Sci. Eng.*, vol. 111, no. 4, pp. 331–336, 1989.
- [22] M. Matthew, C. M. Waits, I. B. Mustafa, and R. Ghodssi, "A rotary microactuator supported on encapsulated microball bearings using an electro-pneumatic thrust balance," *J. Micromech. Microeng.*, vol. 19, no. 9, p. 094007, 2009.
- [23] B. Hanrahan, M. Beyaz, M. McCarthy, C. M. Waits, and R. Ghodssi, "A new performance regime for microfabricated ball bearings," in *Proc. PowerMEMS*, 2010, pp. 191–194.
- [24] B. Hanrahan, J. Feldman, S. Misra, C. M. Waits, P. D. Mitcheson, and R. Ghodssi, "Off-the-shelf MEMS for rotary MEMS," in *Proc. IEEE 25th Int. Conf. Micro Electro Mech. Syst. (MEMS)*, Jan./Feb. 2012, pp. 579–582.
- [25] C. M. Waits, N. R. Jankowski, B. Geil, and R. Ghodssi, "MEMS rotary actuator using an integrated ball bearing and air turbine," in *Proc. Int. Solid-State Sens. Actuators, Microsyst. Conf. (TRANSDUCERS)*, Jun. 2007, pp. 1131–1134.

- [26] L. G. Frechette *et al.*, "High-speed microfabricated silicon turbomachinery and fluid film bearings," *J. Microelectromech. Syst.*, vol. 14, no. 1, pp. 141–152, 2005.
- [27] R. J. Hergert, B. Hanrahan, R. Ghodssi, and A. S. Holmes, "Performance of integrated retainer rings in silicon micro-turbines with thrust style micro-ball bearings," *J. Micromech. Microeng.*, vol. 23, no. 6, p. 065033, 2013.
- [28] D. Chen, M. Sarumi, S. T. S. Al-Hassani, S. Gan, and Z. Yin, "A model for erosion at normal impact," *Wear*, vol. 205, nos. 1–2, pp. 32–39, 1997.
- [29] Y. Oka, M. Matsumura, and T. Kawabata, "Relationship between surface hardness and erosion damage caused by solid particle impact," *Wear*, vols. 162–164, pp. 688–695, Apr. 1993.
- [30] C. Junsheng, Y. Dejie, and Y. Yu, "Application of an impulse response wavelet to fault diagnosis of rolling bearings," *Mech. Syst. Signal Process.*, vol. 21, no. 2, pp. 920–929, 2007.
- [31] L. Zhen, H. Zhengjia, Z. Yanyang, and C. Xuefeng, "Bearing condition monitoring based on shock pulse method and improved redundant lifting scheme," *Math. Comput. Simul.*, vol. 79, no. 3, pp. 318–338, 2008.
- [32] A. H. Epstein, S. A. Jacobson, J. M. Protz, and L. G. Frechette, "Shirtbutton-sized gas turbines: The engineering challenges of micro high speed rotating machinery," in *Proc. 8th Int. Symp. Transp. Phenomena Dyn. Rotating Mach.*, 2000, p. 11.
- [33] North Atlantic Treaty Organization, Research and Technology Organization, Applied Vehicle Technology Panel, and Von Karman Institute for Fluid Dynamics, *Micro Gas Turbines Micro Turbines à Gaz*. Cedex, France: Neuilly-sur-Seine, 2005.



**Jeremy Feldman** received the B.S. degree in electrical engineering from the University of Maryland, College Park, MD, USA, in 2011, with concentrations in microelectronics, nanomaterials, and power systems. His undergraduate research was in high-density thin-film capacitors, optical structured nanomaterials for photovoltaics and sensors, nanolevel security markers, and an extensive study of vibration and wear in rotary microelectromechanical systems (MEMS) devices supported on microball bearing technology. He is currently conducting research at the MEMS Sensors and Actuators Laboratory located at the University of Maryland, and working toward the M.S. degree in systems engineering, with a focus on optical methods for biosensing and biofeedback systems.



**Brendan Michael Hanrahan** received the B.S. degree in ceramic and materials engineering from Clemson University, Clemson, SC, USA, in 2006, and the M.S. and Ph.D. degrees in materials science and engineering from the University of Maryland, College Park, MD, USA, in 2009 and 2013, respectively. Since 2009, he has been a Materials Engineer with the U.S. Army Research Laboratory in the Sensors and Electron Devices Directorate, Adelphi, MD, USA. His research interests include the tribology of high-performance microelectromechanical systems (MEMS) and the development of MEMS components for compact portable power systems.



**Saswat Misra** received the B.S. degree in electrical engineering from the University of Maryland, College Park, MD, USA, in 2013, with concentration in microelectronics. Saswat is currently pursuing the M.S. and Ph.D. degrees from the University of Florida, Gainesville, FL, USA, in electrical engineering. As an undergraduate, Saswat was a Research Assistant at the MEMS Sensors and Actuators Laboratory at the University of Maryland. His research consisted of utilizing vapor phase lubrication for rotary MEMS applications. Saswat was also a summer intern for the United States Army Research Laboratory. His research involved establishing a diamond-etching technique for ion traps.



**Xiao Zhu Fan** received the B.S., M.S., and Ph.D. degrees from the University of Maryland, College Park, MD, USA, in 2006, 2009, and 2013, respectively, with the focus on microfabricated optical and mechanical sensors. Currently, he is a member of the MEMS Sensors and Actuators Laboratory, and his research interests include microsensor integration with a focus on biological nanostructures and biofabrication for selective chemical and biological sensing.



**Christopher Mike Waits (S'01–M'09)** received the B.S. degree in physics from Salisbury University, Salisbury, MD, USA, in 2000, and the M.S. and Ph.D. degrees in electrical engineering from the University of Maryland, College Park, MD, USA, in 2003 and 2008, respectively. He is currently the Technical Assistant to the Director of the Sensors and Electron Devices Directorate at the U.S. Army Research Laboratory, Adelphi, MD. He is also the Team Leader for the Compact Power and Thermal Sciences Teams. His team focuses on developing microcombustion, microfluidics, and thermal-to-electric energy conversion technologies, and new catalyst materials for liquid-fueled soldier and small systems power. His team also focuses on developing two-phase cooling, phase change thermal storage, and advanced thermal management in power electronics. Dr. Waits was the recipient of the Department of the Army's Research and Development Achievement Award for Technical Excellence in 2007, the Physics Excellence Award from Salisbury University in 2000, and the Graduate Assistance in Areas of National Need Fellowship from 2001 to 2003.



**Paul D. Mitcheson (SM'12)** received the M.Eng. degree in electrical and electronic engineering, and the Ph.D. degree from Imperial College London, London, U.K., in 2001 and 2005, respectively. He is currently a Senior Lecturer with the Control and Power Research Group, Electrical and Electronic Engineering Department, Imperial College London. His research interests are energy harvesting, power electronics, and wireless power transfer. He is involved in providing power to applications in circumstances where batteries and cables are not suitable. His research has been supported by the European Commission, Engineering and Physical Sciences Research Council (EPSRC), and several companies. Dr. Mitcheson is a Fellow of the Higher Education Academy.



**Reza Ghodssi** (S'92–M'96–F'14) received the B.Sc., M.Sc., and Ph.D. degrees from the Electrical Engineering Department, University of Wisconsin, Madison, WI, USA, in 1990, 1992, and 1996, respectively. He is currently the Herbert Rabin Distinguished Professor, the Director of the Institute for Systems Research, and the Director of the MEMS Sensors and Actuators Laboratory, Department of Electrical and Computer Engineering, University of Maryland (UMD), College Park, MD, USA. He is also currently with the Fischell Department of Bio-

engineering, the Maryland NanoCenter, the University of Maryland Energy Research Center, and the Materials Science and Engineering Department, UMD. His research interests include the design and development of microfabrication technologies and their applications to micro/nanodevices and systems for chemical and biological sensing; small-scale energy conversion; and harvesting. He has over 115 scholarly journal publications. He is the Coeditor

of the *Handbook of MEMS Materials and Processes* and is an Associate Editor of the *Journal of Microelectromechanical Systems and Biomedical Microdevices*. Dr. Ghodssi is a member of the American Vacuum Society, the Materials Research Society, the American Society for Engineering Education, and the American Association for the Advancement of Science. He was the Chair of the Ninth International Workshop on Micro and Nanotechnology for Power Generation and Energy Conversion Applications, also known as PowerMEMS 2009; the 2012 NSF Workshop on Micro, Nano, Bio Systems; and the Americas Technical Program Committee Chair of the IEEE Sensors 2010–2012 Conferences. He has chaired the committee for the Denice Denton Emerging Leader Award sponsored by the Anita Borg Institute for Women and Technology and Microsoft since 2007. He was the recipient of the 2001 UMD George Corcoran Award, the 2002 National Science Foundation CAREER Award, and the 2003 UMD Outstanding Systems Engineering Faculty Award. Dr. Ghodssi has been selected as a 2014–2015 Distinguished Scholar-Teacher by UMD.